Supporting Information

Full-fiber triboelectric nanogenerator with knitted origami structure for high impact resistance intelligent protection fabric

Guilin Wu[a], Minjie Xu[a], Mengdie Lei[a], Mingmin Liao[a], Yongyue Luo*[d], Yiwei OuYang[a]*, Jize Liu[bc]*, Guangming Cai[a]*

[a].State Key Laboratory of New Textile Materials and Advanced Processing Technologies & School of Textile Science and Engineering, Wuhan Textile University, Wuhan 430200, China

[b].School of Materials Science and Engineering, Hainan University, Haikou 570228, China

[c].National Local Joint Laboratory for Advanced Textile Processing and Clean Production, Wuhan Textile University, Wuhan 430200, China

[d].Agricultural Products Processing Research Institute, Chinese Academy of Tropical, Agricultural Sciences (CATAS), Zhanjiang 524001, China

*Corresponding author: Yiwei OuYang: E-mail address: 2018042@wtu.edu.cn; Jize Liu: E-mail address:ljz@hainanu.edu.cn; Guangming Cai: E-mail address:guangmingcai2006@163.com

Experimental Section

Materials: Polytetrafluoroethylene (PTFE) filaments (diameter 0.2 mm) were acquired from Dongguan SOVETL Special wire and tape Co., Ltd (Dongguan, Guangdong, China). Cu wire (diameter 30 μm, H65, 63.0%-68.5% purity) was obtained from Taizhou Xinxing Meter Material Co., Ltd (Taizhou, Zhejiang, China). Ultrahigh molecular weight polyethylene (UHMWPE) fibers (120 twists, 200 D) were provided by Zhejiang Hengyuan Chemical Fiber Co., Ltd (Hangzhou, Zhejiang, China).

Preparation of UCPMY: The UCPMY could be realized fully on the traditional textile process equipment. Primarily, the UHMWPE@Cu wrap yarn (UCY) was prepared by the equipment capable of continuous and larger-scale manufacturing provided by Zhejiang Jinggong Technology Co., Ltd. The UHMWPE fibers were wrapped by unidirectional in the empty core spindle together with the Cu wires through the guide rods, and were wound onto the parallel sleeve in the opposite direction of the winding rollers via the output rollers for collection. The UHMWPE yarn conveying speed was 3.3 m min^{-1}, the spindle speed was 4000 rpm, and the Cu wire rotation speed was 900 rpm. Then, with the UCY serving as the inner yarn and the PTFE filament acting as the wrapped yarn for protecting the inner yarn, prepared with the aid of an automated braiding machine (Xuzhou Zelong Weaving Machinery Co., Ltd). In brief, the eight bobbins wound with the PTFE filament yarn were divided into two groups that were mounted symmetrically on two sets of spindles rotating clockwise and anticlockwise on the machine bed. The UCY was mounted on an extra spindle under

the machine. During braiding, two groups of PTFE filaments were drawn from the bobbins on the corresponding spindles and reciprocated motion of spindles from one disc to another on the chassis to stably wrap the UCY at the tightening sleeve obtained the UHMWPE@Cu/PTFE multi-layer composite yarn (UCPMY) (Fig. S1).

The weaving of origami structure knitted fabric: Origami structure knitted fabrics were fabricated based on multi-layer structure composite yarn utilizing a hand flat knitting machine (7-gauge, GSJX-HF-42, Guosheng, China). To compare the anti-impact performance of different fabrics, we designed a total of three types of knitted fabrics, incorporating different knitting structures (Fig. S7, S8*)*. Additionally, without origami structure knitted fabric were prepared as a comparison.

Characterization: The surface morphology and microstructure of multi-layer structure composite yarn were measured using SEM (JSM-5600LV, JEOL, Japan). The resistance of the Ag-plated nylon yarn and the surface resistance of the UCPMY were measured using a digital multi-meter (UT89X, UNI-T). Mechanical properties were measured by electronic universal testing machine (EUT2203, Shenzhen SAAS Testing Technology Co., Ltd, China). A flexible testing system (Hunan NanoUp Electronics Technology Co., Ltd) was employed to characterize the conductive stability of UCPMY after stretch, bend, twist, respectively. The low velocity impact tests of the origami structure knitted fabric were performed by a drop weight impact testing machine (In strong, CEAST 9350). The size of the whole specimens was 40 mm × 40 mm, the hammer head weighing 0.977 kg was released from 20 to 50 cm, and the sample was placed on the center of the force sensor. The force sensor and acceleration sensor record the impact force and hammer acceleration during the impact process, respectively. The triboelectric properties were tested using an experimental platform. A commercial

linear mechanical motor (LinMot E1100) was utilized for the periodic contact and separation. A programmable electrostatic meter (Keithley 6514) and a multi-channel acquisition card (DA-ARM1651) were used to measure the *Voc*, *Isc* and *Qsc*. The COSMOL software was used to simulate the spatial potential distribution.

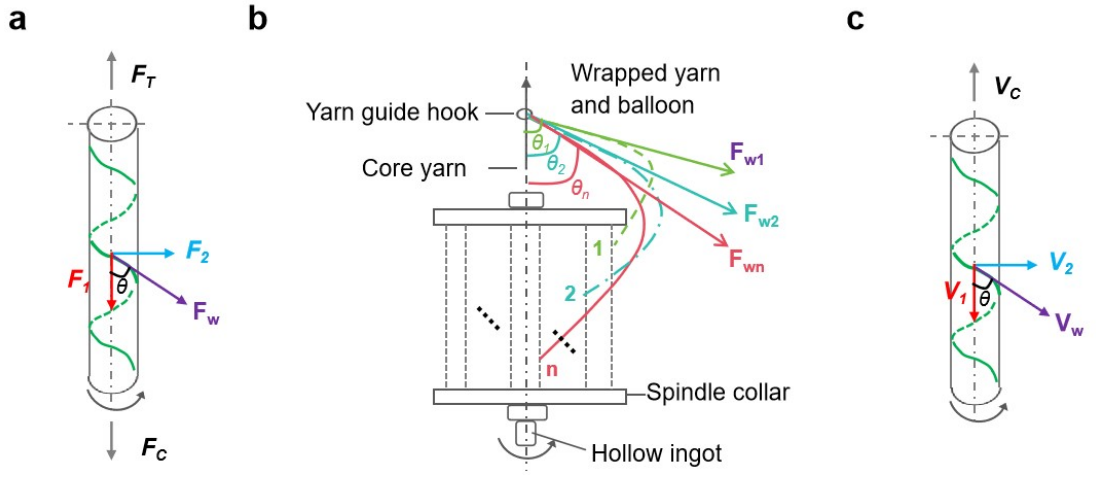

Fig. S1 a) Tension action of outer wrapping yarn on core yarn during inlaying. b) Outer wrapping yarn balloon at different unwinding and peeling points. c) Decomposition of inlaying speed of outer wrapping yarn.

Shown in Fig. S1a, when the outer wrapping yarn was wrapped around the core yarn, it is subjected to the tension F_T of the guide yarn, the tension F_C of the core yarn, and the wrapping tension F_W of the sheath yarn. The tension of the outer wrapping yarn forms an angle θ with the core yarn, and thus can be decomposed into a force F_1 parallel to the core yarn axis and a force F_2 perpendicular to the core yarn axis. Therefore, the relationship between F_W, F_1 and F_2 :

$$F_1 = F_W \cos\theta \qquad (1)$$

$$F_2 = F_W \sin\theta \qquad (2)$$

The perpendicular to axial force F_1 generates a twisting moment, which causes the outer wrapped yarn to wrap around the core yarn. The force F_2 parallel to the axial direction of the core yarn forms the resistance of the sheath yarn to being led out of the spindle tube, and in the steady state, the combined force of the core yarn tension F_C is in equilibrium with the tension F_T of the guide yarn:

$$F_T = F_C + F_1 = F_C + F_W \cos\theta \qquad (3)$$

Fig. S1b shows a schematic diagram of the variation of the shape and length of the balloon on the spindle collar when the unwinding and stripping points of the sheath yarn are located in different yarn layers and at different heights. As the unwinding and stripping point of the outer wrapping yarn on the spindle collar changes with the unwinding and output of the outer wrapping yarn, the length of the balloon section changes continuously, making the shape of the balloon change continuously, which results in the wrapping angle θ of the outer wrapping yarn to the core yarn at the wrapping point changing continuously. As a result, during the preparation process of the composite yarn, the centrifugal, tensile, twisting and frictional forces on the outer wrapping yarns are constantly changing due to the change in wrap angle.

Is depicted in Fig. S1c, V_C is the output speed of the composite yarn, V_W is the line speed of the outer wrapping yarn wrapping the core yarn at the winding point. V_W can be decomposed into an axial component velocity V_1 along the core yarn and a tangential component velocity V_2 along the core yarn. Therefore, the relationship between V_W, V_1 and V_2:

$$V_1 = V_W \cos\theta \tag{4}$$

$$V_2 = V_W \sin\theta \tag{5}$$

V_2 produces the effect of winding the outer wrapping yarn onto the core yarn, whereas V_1 produces the effect of moving the winding point downwards along the core yarn axis (in the opposite direction to the movement of the core yarn). As a result, during the preparation process of the composite yarn, the position of the winding point on the core yarn depends on the magnitude of the output speed of the composite yarn

V_C and V_1, with $V_C > V_1$, the winding point moves upwards along the core yarn, and $V_C < V_1$, the winding point moves downwards along the core yarn. However, the change in the winding point leads to a change in the morphology of the balloon, which in turn causes a change in wrapping angle θ. The speed of V_1 is then varied so that V_1 is numerically infinitely close to V_C, keeping the winding point relatively stable at a certain position in the core yarn.

The line speed of outer wrapping yarn wrapping around the core yarn at the point of wrapping:

$$V_W = \pi dT \qquad (6)$$

where, T is the rotational speed of the outer wrapping yarn, d is the winding diameter of the outer wrapping yarn to the core yarn.

When the winding point relatively stable at a certain position in the core yarn:

$$V_C = \pi dT \cos\theta \qquad (7)$$

Therefore, when the output speed of the composite yarn is kept constant, it is possible to obtain composite yarns with different wrapping angles θ by varying the rotational speed T of the outer wrapping yarn.

Shown in Fig. S2, the low rotation speed of the outer wrapping yarn causes the core to be in loosely and unsteadily wrapped.

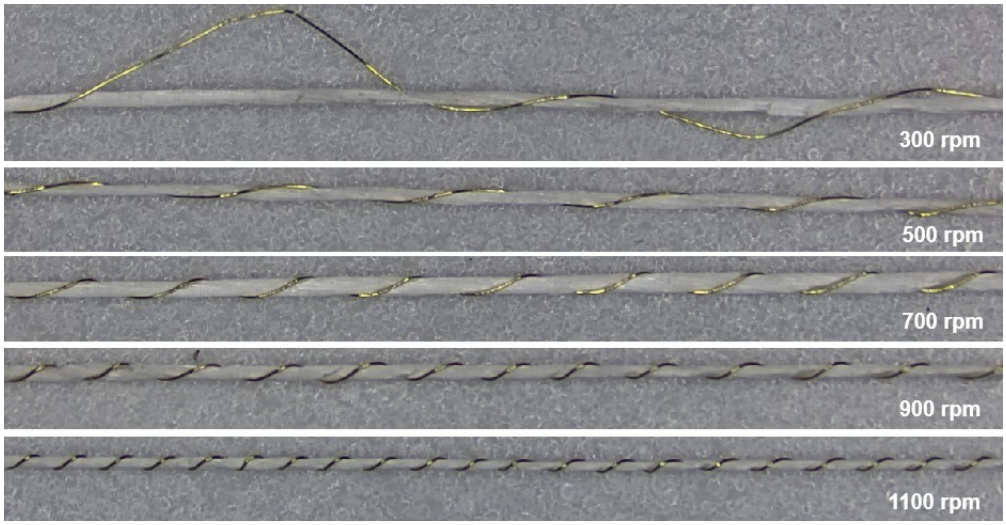

Fig. S2 Image of the UCY fabricated under different wrapping speed.

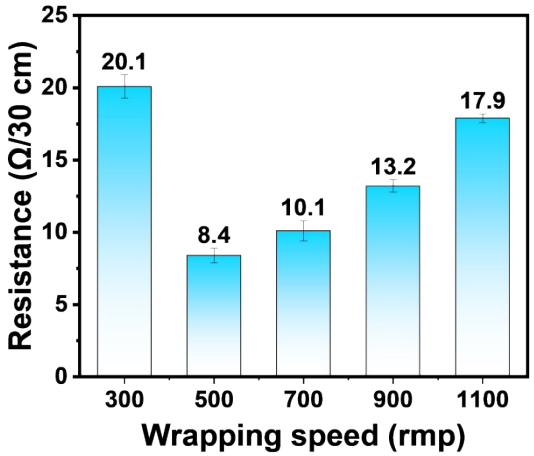

Fig. S3 Resistance of the UCY under different wrapping speed.

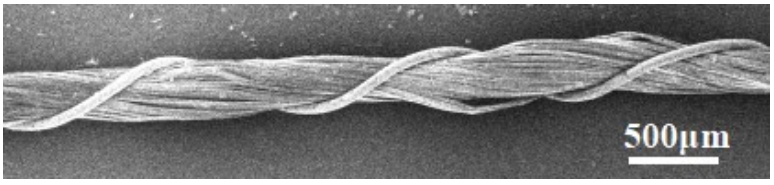

Fig. S4 SEM image of UCY.

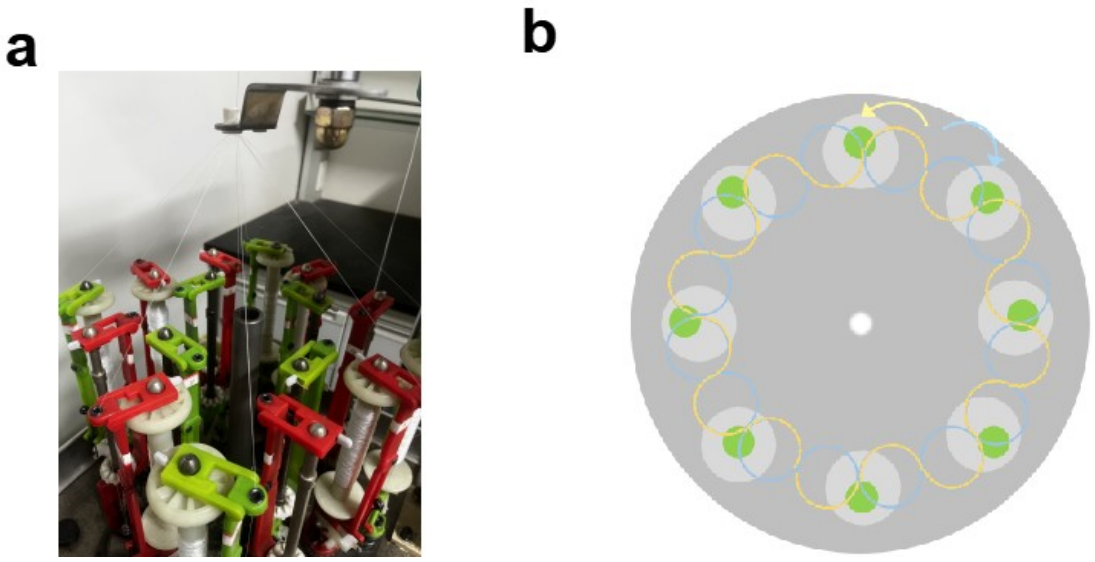

Fig. S5 Fabrication of the UHMWPE@Cu/PTFE multi-layer composite yarn (UCPMY). a) Image of braiding machine. b) Top view of the machine bed and braiding path of the two groups of spindles.

UCPMY was prepared in the automated processing braiding machines composed of a round machine bed on which UCY and PTFE filaments are drawn from the bobbins and then interwoven with each other at the tightening sleeve, and can be easily mass-produced via the top take-up device (Fig. 1e).

Fig. S6 Resistance measurement of 300 mm. a) Cu wire. b) UCY. C) UCPMY. d) Surface resistance of the UCPMY.

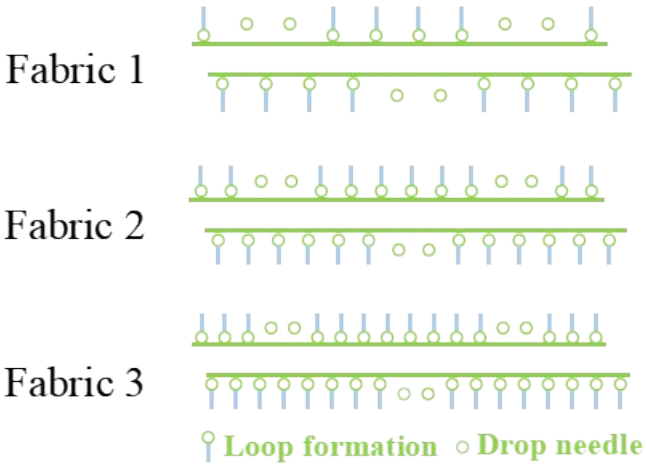

Fig. S7 Woven diagram of different structure OSKFs

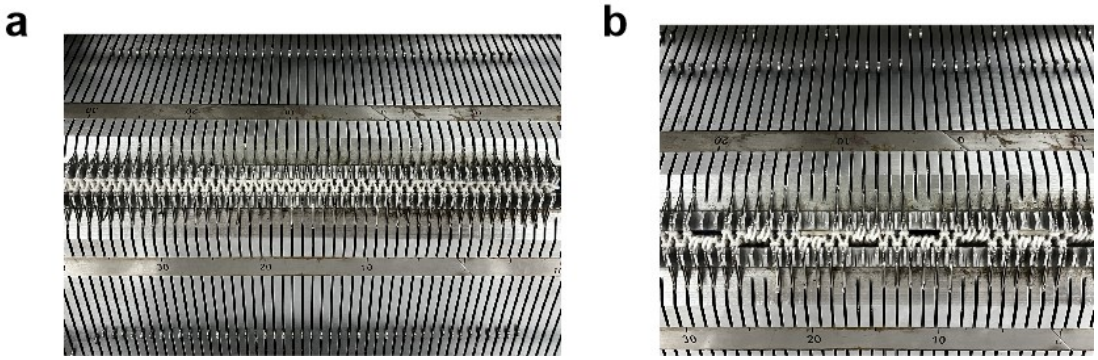

Fig. S8 Process image for the preparation of Fabric 2

The OSKF was fabricated based on multi-layer structure composite yarn utilizing a hand-flat knitting machine. Take Fabric 2 for example: according to the rib stitch lifting the needle, then every 6 knitting stitches, convert the loops of the next 2 knitting needles to the corresponding back and front needle bed positions on the front and back needle beds respectively, and push the needle down to the non-working position. Subsequently, the origami structure knitted fabrics is carried out.

Fig. S9 Image of the as-prepared OSKF.

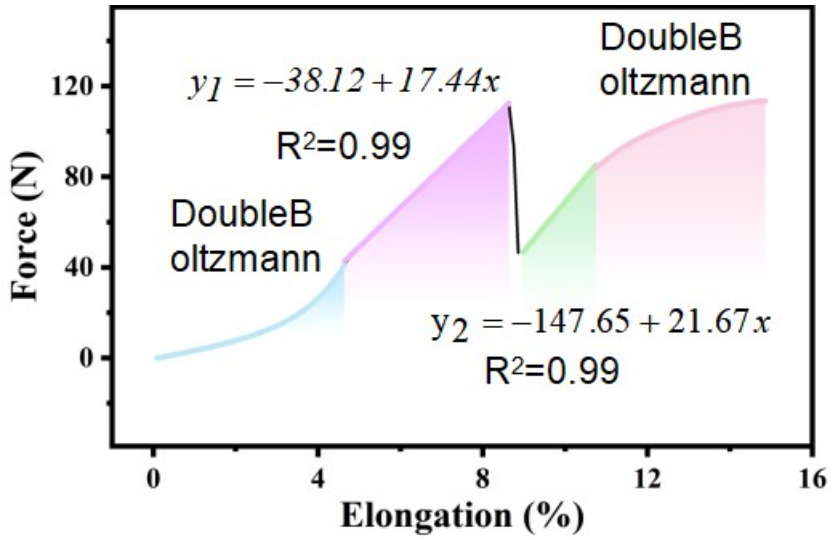

Fig. S10 Load-elongation fitted curves of UCPCY.

Fig. S11 Image of a single UBSY lifting 6.8 kg water.

Fig. S12 Image of thickness test of the OSKF

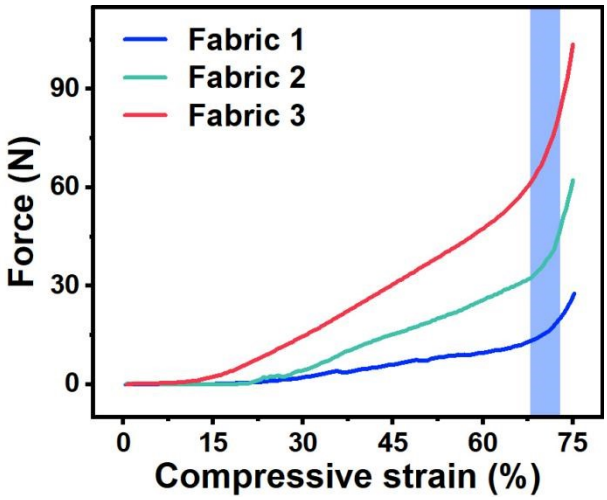

Fig. S13 Compression behavior of different structures of OSKF at compressive strain of 80%.

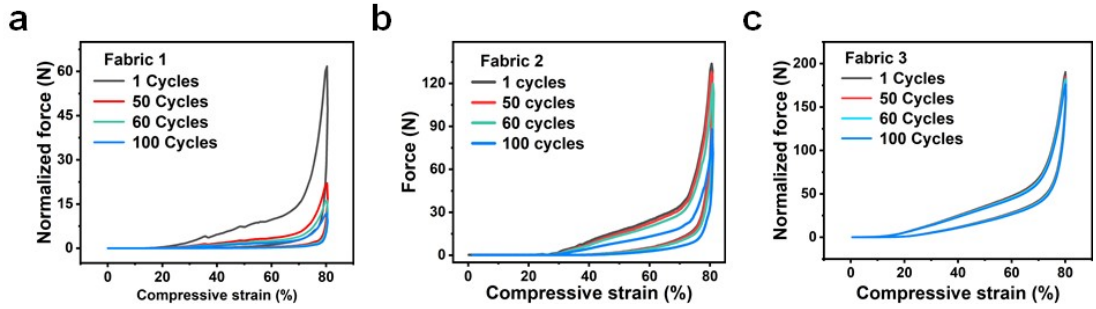

Fig. S14 Cycles compression behavior of OSKFs with different fold size. (a) Fabric 1, (b) Fabric 2, (c) Fabric 3.

As shown in Fig. S14, compression force of Fabric 1 decreased by 73.7% and 80.8% after 50 and 100 compression cycles, respectively; the Fabric 2 decreased by 10.5% and 39.3% after 50 and 100 compression cycles,respectively, whereas that of Fabric 3 maintained it compression force after 100 compression cycles.

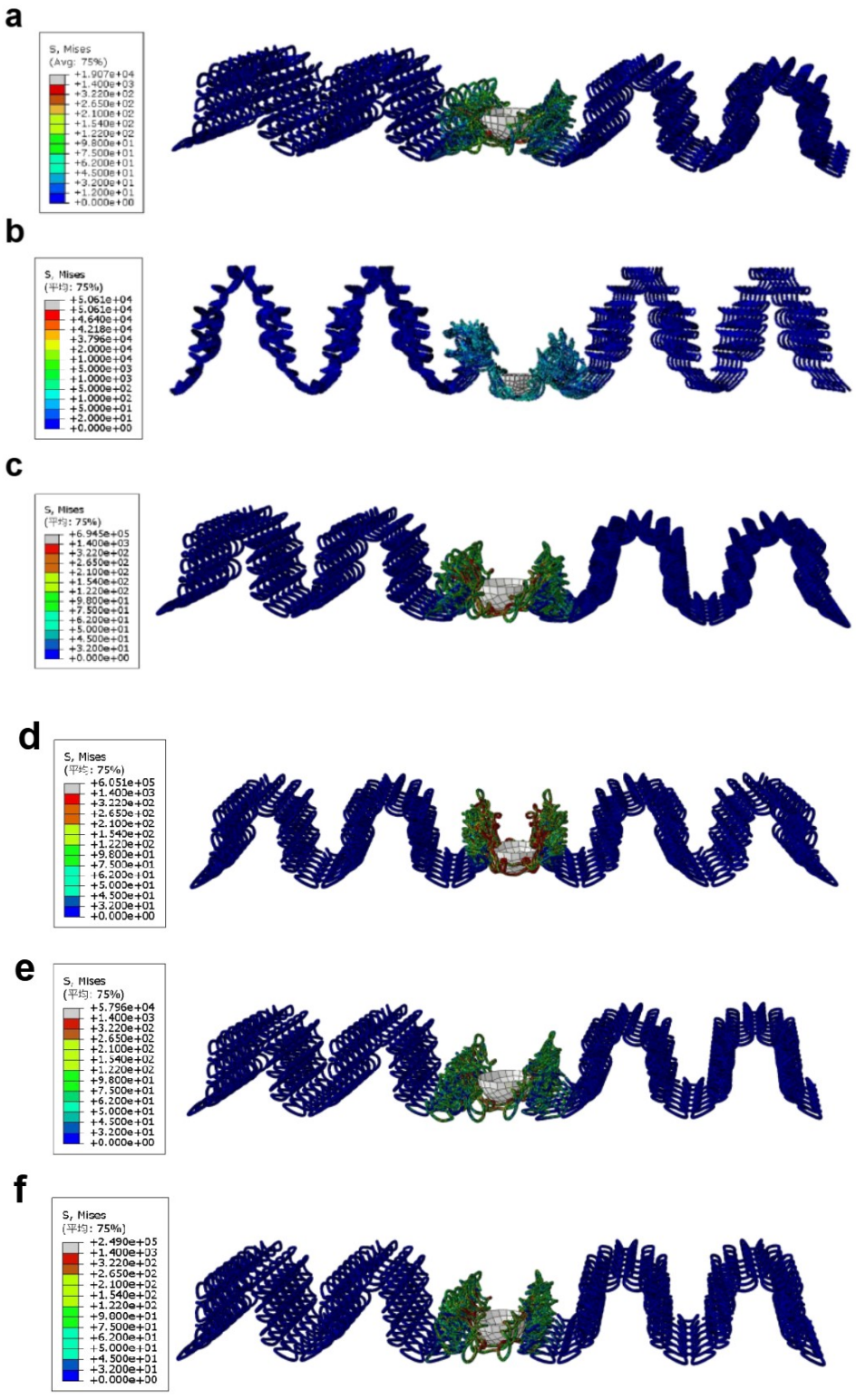

Fig. S15 The simulation results of OSKF with different structures at an impact velocity of 2.801 m/s: (a) F1; (b) F2; (c) F3, The simulation results of Fabric 2 at different impact velocity of 1.981 m/s(d), 2.406 m/s(e) and 3.121m/s (f).

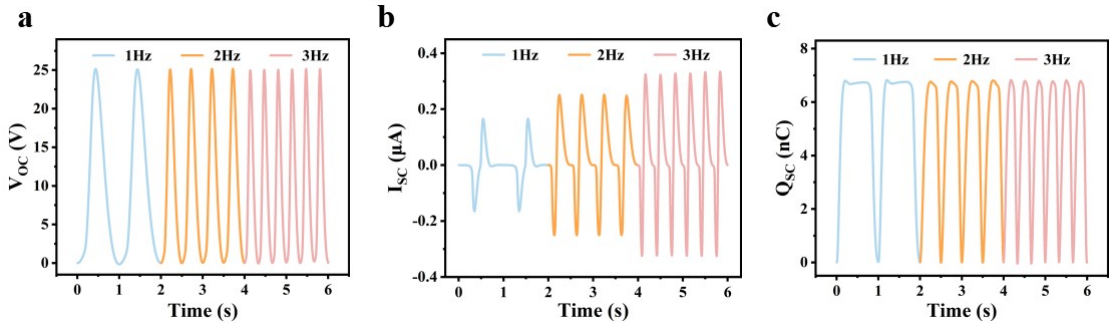

Fig. S16 (a) V_{OC}, (b) I_{SC}, and (c) Q_{SC} of the Fabric 2 based under different loading frequencies (1-3 Hz).

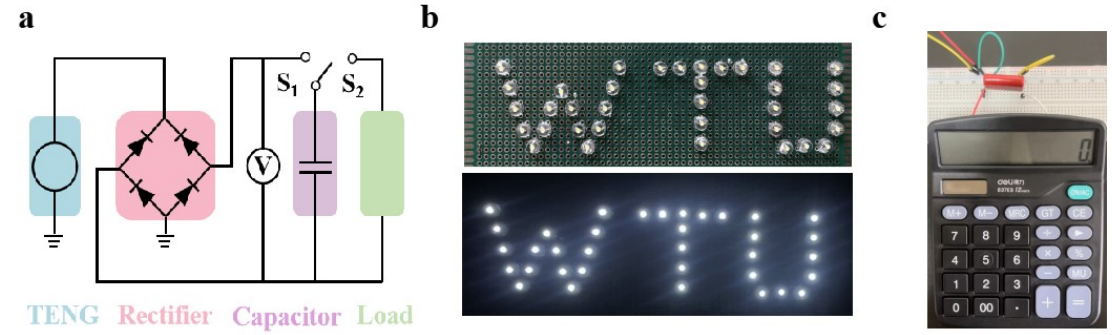

Fig. S17 The capability of OSKF-based TENG to transform biomechanical energy into electrical energy. (a) Equivalent electrical circuit diagram of the TENG used for charging. Image of 35 LEDs (b) and a calculator (c) were lit up by tapping OSKF-based TENG.

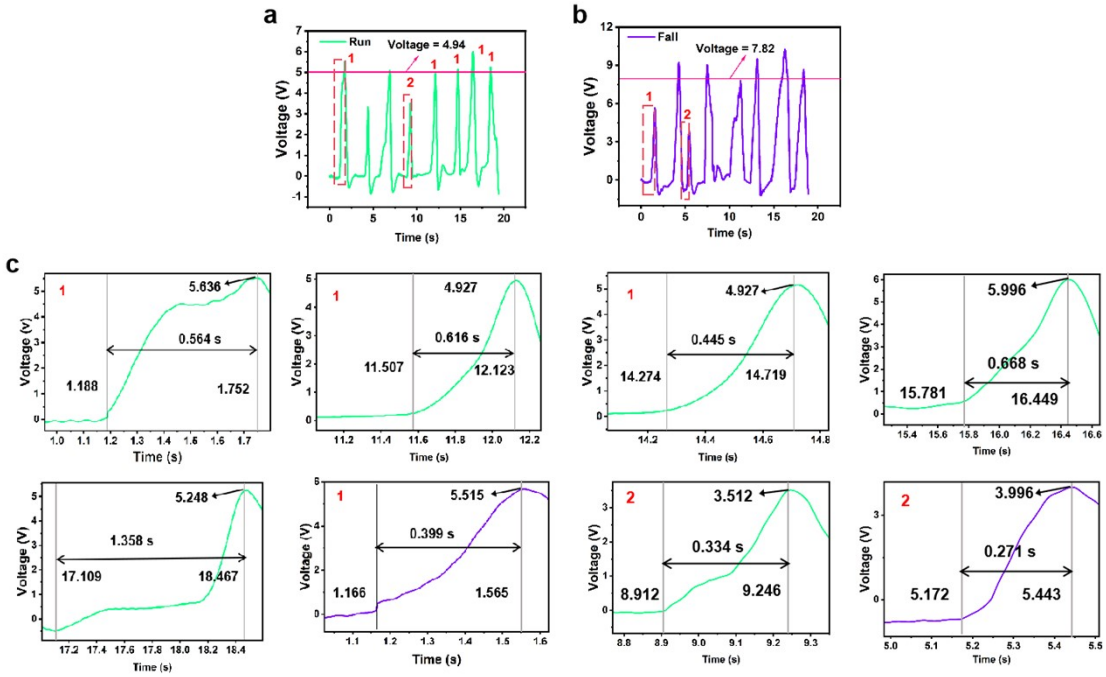

Fig. S18 Characteristic signals contrast of running motion and sudden falls.

Table S1 Performance comparison of the UCPMY with previous reported yarns.

Yarn type	Diameter	Tensile stress	Breaking elongation	Ref.
sheath-core structured CNT@cotton-Ag@nylon yarn	900 μm	20.23 MPa	57.19%	[21]
Anti-UV cotton yarns with antibacterial properties combined with PE yarns	980 μm	1.63 MPa	10.2%	[41]
Assembled core–sheath yarn	6000 μm	2.24 MPa	240.00%	[42]
Hierarchical and coaxial yarn	1900 μm	3.3 MPa	203.00%	[43]
PAN/KCZ/ZnO@PPy nanofiber core-spun yarn	700 μm	14.5 MPa	7.6%	[44]
Fermat-spiral-based energy yarns	471 μm	62.55 MPa	383.00%	[45]
BS@PI core-sheath yarn	520 μm	85.99 MPa	3.12%	[46]
Core-sheath structure piezoelectric yarn	600 μm	87.4 MPa	78.9%	[47]
Spandex/carbon nanotube (CNT)@aramid/aramid (SCAA) yarn	1100 μm	14.21 MPa	160.00%	[48]
Silver-coated nylon and PVDF core-sheath braided yarn	630 μm	158 MPa	145.00%	[49]
UCPMY	820 μm	219.18 MPa	14.86%	This work

Table S2 The corresponding relationship between the release height of the drop hammer and the impact speed and kinetic energy.

Release height	Impact speed	Kinetic energy
20 cm	1.981 m/s	4.476 J
30 cm	2.426 m/s	6.701 J
40 cm	2.801 m/s	8.932 J
50 cm	3.132 m/s	11.168 J